Geologie en Mijnbouw **73:** 169–172, 1994.

The stress tensor in the Rhine Graben area derived from earthquake focal mechanisms (extended abstract)

T. Plenefisch & K.-P. Bonjer
Geophysical Institute, Karlsruhe University, Hertzstrasse 16, 76187 Karlsruhe, Germany

Received 8 June 1993; accepted 16 September 1993

Key words: focal mechanism inversion, stress tensor

Focal mechanisms of microearthquakes are used to study the stress tensor in the Rhine Graben and adjacent areas. To reveal the stress tensor we apply the inversion method of Gephart & Forsyth (1984). Following their suggestion we perform the approximate method in an initial wide-ranging grid search and subsequently the exact method in a more narrow range around the minima of the preceding analysis.

Altogether 83 well-constrained fault plane solutions (strike-slip, normal and thrust mechanisms) of crustal earthquakes are used as our database. The nodal planes of the selected earthquakes are fixed with an accuracy better than 10 degrees. The locations of the earthquakes are spread from the southernmost end of the Rhine Graben up to the Lower Rhine Embayment (Fig. 1). To investigate lateral differences in the stress tensor, the whole dataset is divided into three subsets. The first dataset comprises fault plane solutions from events located in the northern Alpine foreland (Pavoni 1987; Deichmann 1990). Events of the southern Rhine Graben and the Black Forest region build the second dataset (Bonjer 1992). Including the well-documented fault plane solution of the 1992 Roermond earthquake (Ahorner 1992; Paulssen et al. 1992; Braunmiller et al. 1994a, b), the third dataset covers the region of the northern Rhine Graben, the Rhenish Massif and the Lower Rhine Embayment (Ahorner et al. 1984).

The results of the inversion (approximate method) are shown in equal area projection of the positions of the greatest (σ_1) and the least (σ_3) principal stress axes (Fig. 2). Big dots represent directions of principal stress axes fulfilling the 68% confidence criterion for one-norm misfits (Parker & McNutt 1980). This means that for these data the corresponding stress tensors require only very small rotations of the fault planes to match observed and predicted slip vectors.

In all datasets the family of the best stress tensors (Fig. 2) is characterized by a stable σ_3-direction, being horizontal to subhorizontal with a strike of about 240° (60° resp.). The σ_1- as well as the σ_2-axes (not shown here) are located in a vertical plane with a strike of about 150°. Depending on the dataset used, σ_1 and σ_2 alternately are close to vertical or horizontal orientations, or somewhere in between. For the southern Rhine Graben a strike-slip regime is found, whereas for the northern Rhine Graben and northern Switzerland both an extensional and a strike slip regime are compatible with the data. The results of the inversion show clearly that a compressional regime is not compatible with the results of the inversion.

The best tensor of each dataset revealed by the exact method is given in Table 1. Within 20 degrees the azimuths of the horizontally oriented principal stress axes agree with the results of the inversions of Carey & Mercier (1992). However, the resolved regimes differ. Carey & Mercier found a strike-slip regime for the northern Alpine foreland and an extensional regime for the southern Rhine Graben, the northern Rhine Graben and the Rhenish Shield. The main reason for these differences is the exclusion of thrust events in their analysis.

For all our datasets, the relative stress magnitude R ($R = (\sigma_2 - \sigma_1)/(\sigma_3 - \sigma_1)$) has a value around 0.5, which means that the deviatoric components of σ_1 and σ_3 are of the same magnitude but have opposite signs. The direction of the maximum horizontal stress of about 150° is in good agreement with the results of regional in-situ stress measurements and the orientation of the general maximum horizontal stress component, S_{Hmax}, in western Europe (e.g. Müller et al. 1992).

A counterclockwise rotation of 35° of the plane built by σ_1 and σ_2 and the strike direction of σ_3 can be

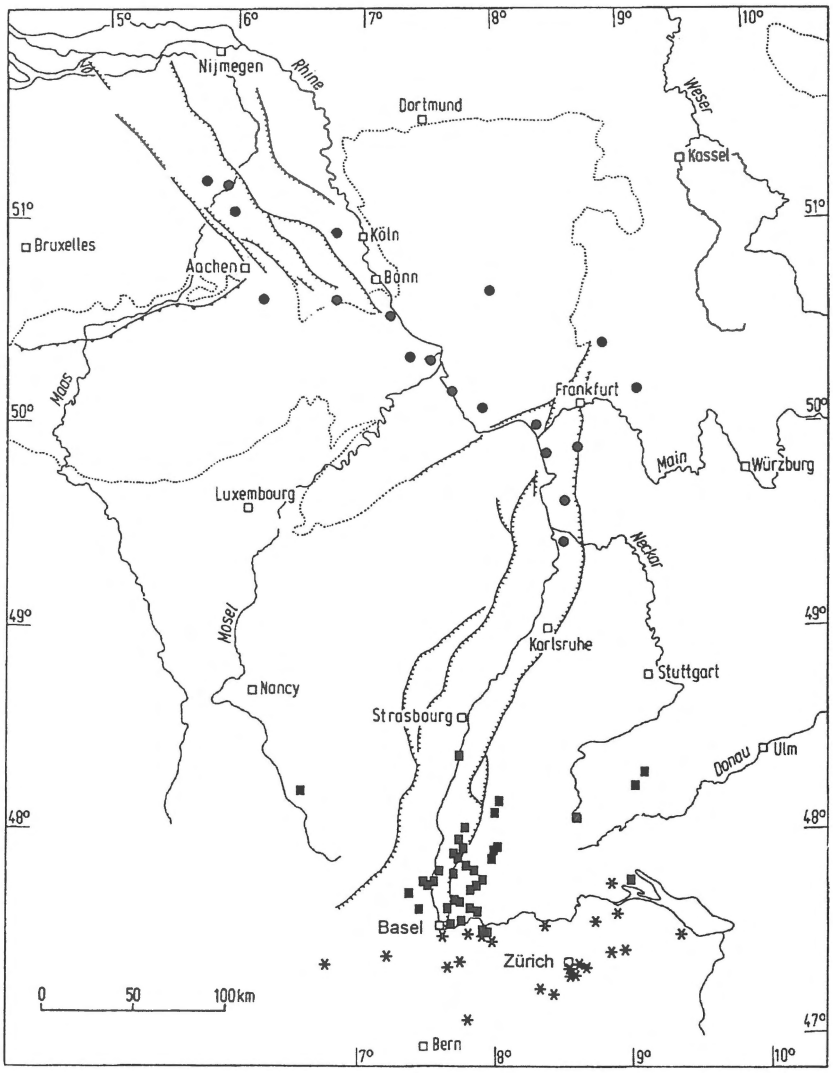

Fig. 1. Tectonic sketch map (after Ahorner et al. 1984) and locations of earthquakes used in the inversions (★ northern Alpine foreland, ■ southern Rhine Graben, ● northern Rhine Graben, Rhenish Massif (dotted outline) and Lower Rhine Embayment).

Table 1. Principal stress axes (σ_1, σ_2 and σ_3) and the stress ratio (R) of the best stress tensors calculated with the exact method

Dataset	σ_1		σ_2		σ_3		R-value
	azimuth	dip	azimuth	dip	azimuth	dip	
N Alpine foreland	105°	76°	1°	4°	270°	14°	0.3
S Rhine Graben	150°	0°	60°	86°	240°	5°	0.5
N Rhine Graben, Rhenish Massif and Lower Rhine Embayment	339°	60°	135°	28°	230°	10°	0.5

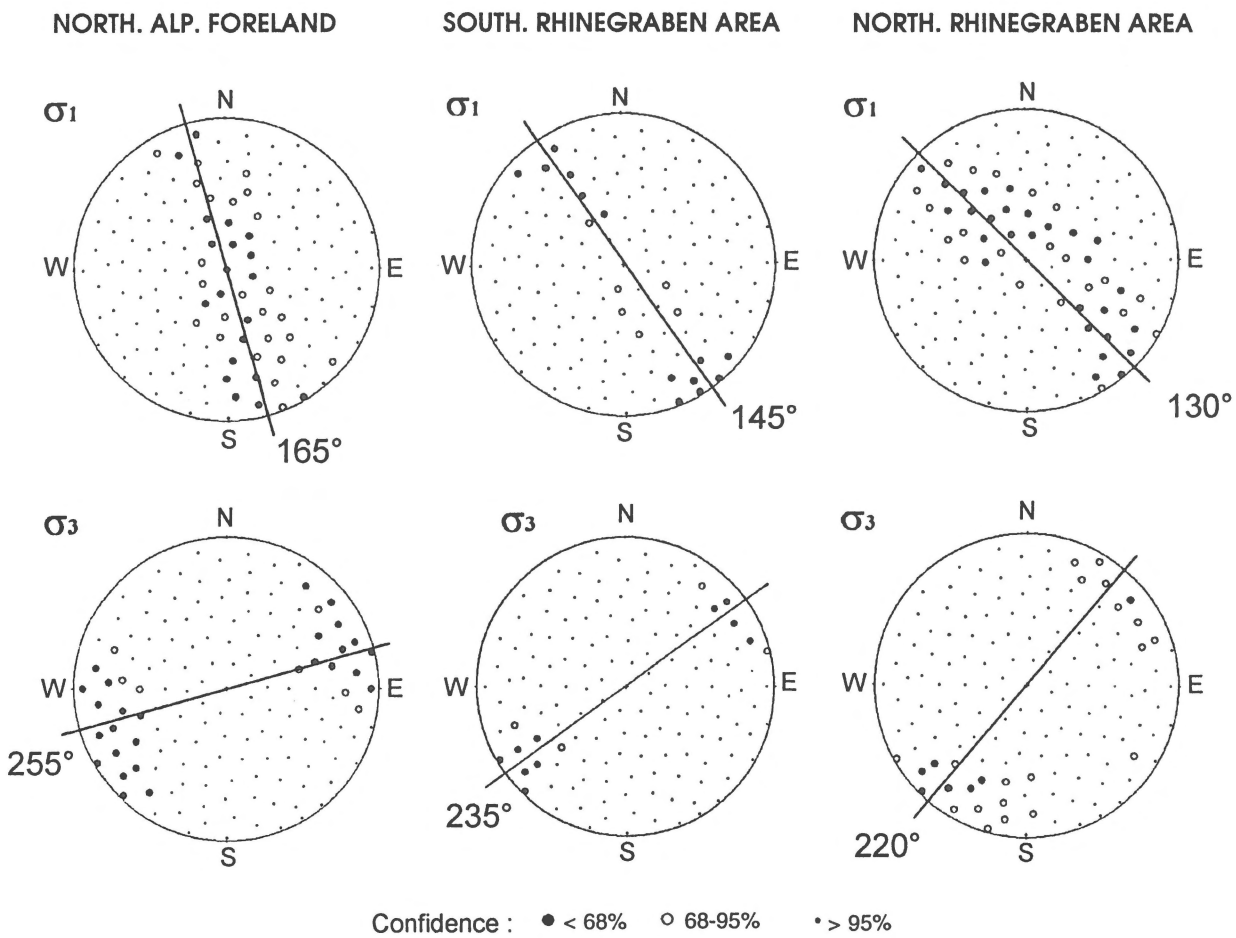

Fig. 2. Lower hemisphere equal area projection showing the σ_1- and σ_3-axes tested in the inversion with the approximate method. Different symbols represent axes of different confidence or misfit, respectively. Straight lines symbolize the average directions where the stress axes exhibit small misfit angles.

observed when comparing the results of the different subsets from south to north.

So far our analysis takes into account only geometrical constraints. With the inference of frictional constraints we will try to get more restrictions on our results and to solve some of the remaining ambiguities in the type of the regional tectonic regimes.

Acknowledgements

We thank J.W. Gephart for providing us with his stress inversion programs. Two anonymous reviewers were very helpful in improving this paper. We are especially grateful for M.C. Oncescu for fruitful discussions and helpful advice. Thanks are also due to T. Dahm for critically reading the manuscript. This study has been supported by the German Research Association (SFB 108). Contribution No. 406 (SFB 108) Geophysical Institute, University of Karlsruhe.

References

Ahorner, L. 1992. Das Erdbeben bei Roermond am 13. April 1992 und die daraus zu ziehenden Lehren für das Erdbebengefährdungspotential im Rheinland – Deutsche Geophys. Ges. Mitt. 1–2: 51–57

Ahorner, L., B. Baier & K.-P. Bonjer 1984 General pattern of seismo tectonic dislocation and the earthquake-generating field in central Europe between the Alps and the North Sea. In: H.J. Illies, K. Fuchs, K. von Gehlen, H. Mälzer, H. Murawski & A. Semmel (eds): Plateau Uplift – The Rhenish Massif – A Case History – Springer Verlag, Heidelberg: 187–197

Bonjer, K.-P. 1992 The southern part of the Upper Rhinegraben area: seismicity and seismic dislocation pattern at the eastern masterfault system – SFB Berichtsband 108: 985–1032

Braunmiller, J., T. Dahm & K.-P. Bonjer 1994a Source mechanism of the 1992 Roermond earthquake from surface wave inversion of regional data – Geophys. J. Int., 116: 663–672

Braunmiller, J., T. Dahm & K.-P. Bonjer 1994b Source mechanism of the 1992 Roermond earthquake, the Netherlands, from inversion of regional surface waves (extended abstract) – Geol. Mijnbouw, this issue

Carey, E. & J.L. Mercier 1992 Regional state of stress, fault kinematics and adjustments of blocks in a fractured body of rock: application to the microseismicity of the Rhine graben – J. Struct. Geol. 14: 1007–1017

Deichmann, N. 1990 Seismizität der Nordschweiz 1987–1989, und Auswertung der Erdbebenserie von Günzburg, Läufelfingen und Zeglingen – NAGRA TB 90-46, 56 pp

Gephart, J.W. & D.W. Forsyth 1984 An improved method for determining the regional stress tensor using earthquake focal mechanism data: Application to the San Fernando earthquake sequence – J. Geophys. Res. 89: 9305–9320

Müller, B., M.L. Zoback, K. Fuchs, L. Mastin, S. Gregersen, N. Pavoni, O. Stephansson & C. Ljungren 1992 Regional patterns of tectonic stress in Europe – J. Geophys. Res. 97: 783–803

Parker, R.L. & M.K. McNutt 1980 Statistics for the one-norm misfit measure – J. Geophys. Res. 85: 4429–4430

Paulssen, H., B. Dost & T. van Eck 1992 The April 13, 1992 earthquake of Roermond (The Netherlands); first interpretation of the NARS seismograms – Geol. Mijnbouw 71: 91–98

Pavoni, N. 1987 Zur Seismotektonik der Nordschweiz – Eclogae Geol. Helv. 80: 461–472